scientific reports

Check for updates

OPEN

Biological and computer-aided evaluation of 3-methoxy-13α-estrone-16α-diphenylphosphine oxide as a new antiestrogenic agent

Sándor Bartha[1], Péter Germán[1], Noémi Bózsity[1], László G. Puskás[2], Rita Börzsei[3], Csaba Hetényi[3], István Zupkó[1], Erzsébet Mernyák[4] & Renáta Minorics[1]✉

Breast cancer, a leading cause of cancer-related mortality, often depends on estrogen receptor alpha (ERα) signaling for progression. This study evaluates [(3-methoxy-17-oxo-13α-estra-1,3,5(10)-trien-16α-yl)methyl]diphenylphosphine oxide (EDPO), a recently published organophosphorus 13α-estrone derivative, as a potential antiestrogenic agent. In our previous study, EDPO showed substantial antiproliferative effect against T47D breast cancer cells and UPCI-SCC-131 oropharyngeal squamous cell carcinoma cells, with IC_{50} values of 7.2 µM and 5.3 µM, respectively. Using in silico, in vitro, and in vivo methods, EDPO demonstrated robust antiestrogenic activity comparable to that of fulvestrant. Molecular docking confirmed EDPO's effective binding to the ERα ligand-binding domain, disrupting estrogen signaling. In vitro, EDPO inhibited estrogen-mediated transcriptional activity, induced G1-phase cell cycle arrest, and significantly reduced the invasive capacity of breast cancer cells, as well as the extent of cell migration both in breast and oropharyngeal carcinoma cells. In vivo uterotrophic assay on immature rats revealed EDPO's ability to mitigate estrogen-induced uterine growth, validating its antiestrogenic effects. Moreover, in a murine triple-negative breast cancer (TNBC) model, EDPO significantly inhibited tumor growth, likely through immunomodulatory mechanisms that altered the tumor microenvironment. These findings highlight EDPO's multifaceted actions, combining antiestrogenic, antiproliferative, and antimetastatic effects. This study positions EDPO as a promising hit molecule for both ERα+ breast cancer and TNBC, addressing key challenges in current endocrine therapies and offering new avenues for breast cancer treatment.

Keywords 13α-estrone, Estrogen receptor alpha, Antiestrogen, Breast cancer, Antiproliferative, Antimetastatic

Breast cancer is the most frequently diagnosed type of cancer (accounting for approximately 1 out of 4 cases) and now, surpassing lung cancer, is the leading cause of death among women worldwide[1]. Malignant breast tumors are initially classified based on their expression of estrogen receptor (ER), progesterone receptor (PR), and human epithelial growth factor receptor 2 (HER2). Receptor positivity is an important prognostic factor, approximately 70% of breast tumors are ERα+, which are considered the most favorable in terms of survival[2]. Treatment options include selective estrogen receptor modulators (SERMs), e.g. tamoxifen; selective estrogen receptor degraders (SERDs), for example, fulvestrant; aromatase inhibitors, such as exemestane, commonly known as antiestrogens, in both the early-stage and metastatic settings[3,4]. Although survival rates of breast cancer patients have improved in recent years, acquired resistance to treatment, relapsing, and metastasis formation remain significant challenges, necessitating the exploration of novel treatment strategies.

[1]Institute of Pharmacodynamics and Biopharmacy, University of Szeged, Eötvös u. 6, Szeged H- 6720, Hungary. [2]Avidin Ltd, Alsó kikötő sor 11/D, Szeged H-6726, Hungary. [3]Pharmacoinformatics Unit, Department of Pharmacology and Pharmacotherapy, Medical School, University of Pécs, Szigeti út 12, Pécs H-7624, Hungary. [4]Department of Pharmacognosy, University of Szeged, Eötvös u 6, Szeged H-6720, Hungary. ✉email: kanizsaine.minorics.renata@szte.hu

Targeting estrogen signaling at various stages has proven to be a challenging but effective method for curing ERα+ breast cancer[5]. SERMs, such as tamoxifen and raloxifene, have revolutionized breast cancer therapy by selectively blocking ERs in breast tissue, thereby impeding estrogen-driven cancer cell proliferation. Recent experimental SERMs, such as bazedoxifene or lasofoxifene, have shown promise in preclinical breast cancer models due to their potent antiestrogenic effects on breast tissue, offering hope for future therapeutic options[6,7]. Additionally, steroid sulfatase (STS) inhibitors have emerged as a novel class of therapeutic agents by preventing the conversion of sulfated steroid precursors into active estrogens, thus reducing estrogen levels and mitigating tumor growth[8].

Fulvestrant, a pure antiestrogen or SERD, represents another critical advancement in the field. Unlike traditional SERMs, fulvestrant binds to the ERα and promotes its degradation, leading to a more complete inhibition of estrogen signaling[9]. Since its approval in 2002, fulvestrant has become a standard treatment for postmenopausal women with advanced ERα+ breast cancer, particularly those who have progressed on other endocrine therapies[10]. Fulvestrant remains the gold standard SERD and a cornerstone of therapy for advanced ERα+ breast cancer, with its clinical efficacy establishing it as the benchmark for newer agents. However, limitations such as low bioavailability and intramuscular administration, together with reduced activity against tumors harboring ESR1 mutations, underscore the need for improved options. These challenges have driven the development of next-generation SERDs that aim to preserve the therapeutic strengths of fulvestrant while offering superior pharmacokinetics and efficacy against resistant disease. An overview of fulvestrant in comparison with clinically available and emerging SERDs is presented in Table 1.

Ongoing research continues to expand the arsenal of SERDs, exploring both steroidal and non-steroidal candidates. Recently, we have reported the phospha-Michael addition reactions of 3-methyl or –benzyl ether of the core-modified 16-methylene-13α-estrone[17]. The conformational change, as the result of the epimerization of natural estrone at C-13, leads to suppressed estrogenic activity[18]. The markedly decreased hormonal behavior allows the development of 13α-estrone derivatives with other, selective biological properties[19–21]. Certain D-ring-modified derivatives displayed anticancer activity against gynecological human cancer cell lines. Based on these promising results, the 12 tertiary phosphine oxide derivative diastereomers of 13α-estrone (with a newly formed chiral center at C-16) were subjected to antiproliferative effect assessment against a panel of adherent cell lines of gynecological and oropharyngeal origin using standard MTT assay. One of the derivatives, [(3-methoxy-17-oxo-13α-estra-1,3,5(10)-trien-16α-yl)methyl]diphenylphosphine oxide (EDPO) exerted a substantial inhibitory effect on the proliferation of T47D (IC_{50} = 7.2 μM) and UPCI-SCC-131 (IC_{50} = 5.3 μM) cells, moderate inhibitory effect on MCF-7 (IC_{50} = 13.7 μM) cells, and relatively low inhibitory effect on MDA-MB-231 (IC_{50} = 23.5 μM) triple-negative breast cancer cells. Notably, EDPO displayed up to 1.50-, 2.83- and 3.85-fold greater potency against MCF-7, T47D and UPCI-SCC-131 cells, respectively, in comparison to its effect on non-cancerous mouse fibroblast cells (NIH/3T3; IC50 = 20.4 μM)[17]. These experimental findings demonstrate that EDPO selectively inhibits the proliferation of ERα+ cancer cells. Based on these results, where we observed a negative correlation between ERα-positivity and the IC_{50} value of EDPO measured on the breast cancer cell lines, we hypothesized that our compound may exert its effect through the ERα-signaling. The objective of the current study was to elucidate the proposed antiestrogenic mechanism of action of our test compound through a comprehensive series of in silico, in vitro, and in vivo experiments. This investigation may further broaden the pharmacodynamic repertoire of the previously characterized 13α-estrone derivatives, which are acknowledged as aromatase, 17β-hydoxysteroid dehydrogenase 1 and/or STS inhibitors[22,23], by introducing an additional novel mechanism of action. Furthermore, the results of our studies may draw attention to the therapeutic potential inherent in the derivatives of 13α-estrone.

Materials and methods

Chemicals and cell cultures

The two tested organophosphorus 13α-estrone derivatives, EDPO and [(3-benzyloxy-17-oxo-13α-estra-1,3,5(10)-trien-16α-yl)methyl]diphenylphosphine oxide (3-BEDPO; Fig. 1) were synthesized by Mernyák et al. as described previously[17]. For all in vitro experiments, 10 mM stock solutions of the test compounds were prepared with dimethyl sulfoxide (DMSO). Adherent carcinoma cell lines of human origin, UPCI-SCC-131 (ACC-668 from DSMZ - German Collection of Microorganisms and Cell Cultures GmbH, Braunschweig, Germany) and T47D (85102201 from European Collection of Authenticated Cell Cultures, Salisbury, UK) were cultured and maintained in a minimum essential medium (Capricorn Scientific GmbH, Ebsdorfergrund,

Drug	Structure	EC_{50} of ERα degradation (nM)	Mechanism of action	Effective in ESR1 mutation	Administration
Fulvestrant[11]	steroidal	9.3	degrader/ down-regulator	no	im. injection
Elacestrant[12]	non-steroidal	0.6	degrader/ modulator	yes	oral
Amcenestrant[13]	non-steroidal	0.2	degrader/ down-regulator	yes	oral
Giredestrant[14]	non-steroidal	0.05	degrader/ down-regulator	yes	oral
Camizestrant[15]	non-steroidal	0.2	degrader	yes	oral
Imlunestrant[16]	non-steroidal	3.0	degrader	yes	oral

Table 1. Comparison of clinically available and experimental SERDs.

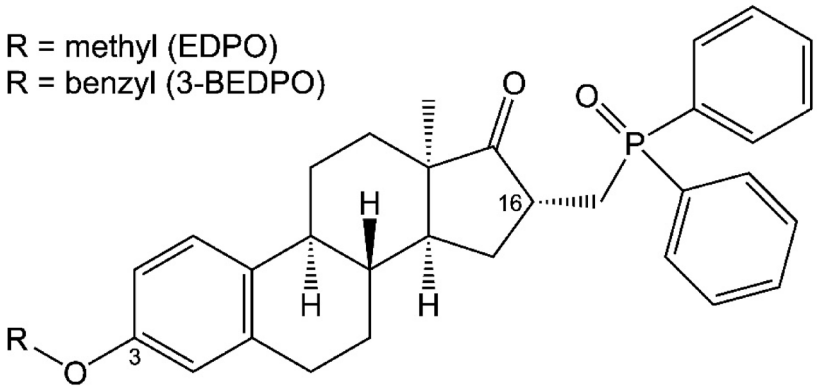

Fig. 1. Chemical structures of [(3-methoxy-17-oxo-13α-estra-1,3,5(10)-trien-16α-yl)methyl] diphenylphosphine oxide (EDPO) and [(3-benzyloxy-17-oxo-13α-estra-1,3,5(10)-trien-16α-yl)methyl] diphenylphosphine oxide (3-BEDPO).

Germany) supplemented with 10% fetal bovine serum (FBS, Capricorn Scientific GmbH, Ebsdorfergrund, Germany), 1% non-essential amino acids, 1% L-glutamine and 1% antibiotic-antimycotic mixture. Moreover, the T47D-KBluc cell line (CLR-2865™, ATCC, Manassas, VA, USA) was used to determine the antiestrogenic effect. Cells were cultured in phenol red-free RPMI (Thermo Fisher Scientific Inc., Waltham, MA, USA) medium supplemented with 10% FBS, 1% non-essential amino acids, 1% L-glutamine, and 1% antibiotic-antimycotic mixture. All cell lines were incubated at 37 °C in humidified atmospheric air containing 5% CO_2. All media and reagents, unless otherwise indicated, were purchased from Merck KGaA (Darmstadt, Germany).

In silico human estrogen receptor binding

Ligand preparation

The investigated 13α-estrone derivative ligands (EDPO and 3-BEDPO) were built with the Maestro program package (Schrödinger Release 2025-1: Maestro, Schrödinger, LLC, New York, NY, 2025). In the meantime, raloxifene and fulvestrant were cut from their experimental complexes obtained from the Protein Data Bank (PDB code: 7kbs, 4j03, respectively)[24–26]. All ligand structures were minimized by the semiempirical quantum chemistry program package, MOPAC (MOPAC2016, James J. P. Stewart, Stewart Computational Chemistry, Colorado Springs, CO, USA, http://OpenMOPAC.net (2016)), with PM7 parametrization[27]. The gradient norm was set to 0.001. Force calculations were applied to the energy-minimized structures used for docking calculations, and force constant matrices were positive definite.

Target preparation

Throughout the in vitro and in vivo experiments, fulvestrant was used as reference molecule, however, its complex with the human estrogen receptor alpha ligand binding domain (hERα LBD) is not available in atomic resolution. Therefore, the raloxifene-bound conformation of hERα LBD was used as the target in this study. The experimental structure was obtained from the Protein Data Bank (PDB code: 7kbs)[25]. "B" conformation residues, water molecules, ions, and ligands were removed from the original experimental structure, and missing residues and atoms were added. After capping N- and C-terminals, a two-step energy-minimization process was performed by GROMACS[28] using AMBER-ILDN force field[29]. The target was positioned at the center of a cubic box, maintaining a 10 Å distance between the box boundaries and the solute atoms. The simulation box was filled with TIP3P[30] explicit water molecules and counterions to neutralize the total charge of the system. The convergence threshold of the first (steepest descent) and second (conjugate gradient) step of minimization was set to 100 and 10 kJ mol^{-1} nm^{-2}, respectively.

Docking calculations

Docking calculations were performed with AutoDock 4.2.6[31] using the minimized and equilibrated ligand and target structures. The searching region on the target included the binding pocket area of raloxifene, determined experimentally. Grid box was generated by AutoGrid 4.2.6[31] with dimensions of 70 × 56 × 70 grid points and a spacing of 0.375 Å. It was centered on raloxifene to encompass its binding pocket, with an additional 10 Å extension along all axes to ensure sufficient space for even the longest ligand to adopt the optimal docking pose. AutoDockTools[31] was used to assign Gasteiger-Marsilli partial charges to both the ligand and the receptor atoms, besides a united-atom representation for non-polar moieties. The receptor was treated rigidly, however, flexibility was allowed at all active torsions of the ligands. Lamarckian genetic algorithm was used for global search. 10 docking runs were performed for all ligands. Ligand conformations were ranked by the corresponding calculated interaction energy values and subsequently clustered using a tolerance of 3.5 Å root mean square deviation (RMSD) between cluster members. The rank 1 was analyzed and selected as the representative structure for each ligand. Target residues interacting with the ligand in a 3.5 Å cut-off distance were determined and further analyzed.

Luciferase reporter assay

The in vitro antiestrogenic activity of our test compound was determined by utilizing T47D-KBluc, an ERα+ cell line stably transfected with a ERE-luciferase reporter gene cassette[32]. Cells were seeded onto 96-well microplates in a density of 50.000 cells/well. After 72 h of incubation, the medium was changed to phenol red-free RPMI, containing 10% charcoal-stripped FBS. This step was repeated for another four consecutive days in order to deplete the intracellular estrogen abundance. On the ninth day, the cells were treated with 3.5×10^{-11} M E2 and fulvestrant (1×10^{-12} – 5×10^{-8} M) or the test compounds (4×10^{-7} – 6×10^{-5} M). After 24 h of incubation, the supernatant was removed from the wells, and ONE-Glo™ firefly luciferase reagent was added according to the manufacturer's instructions (Promega Corp., Madison, WI, USA). Following a 5-minute incubation period, the luciferase enzyme activity was measured by a luminometer (FLUOstar OPTIMA, BMG Labtech GmbH, Ortenberg, Germany). Each concentration was assayed in triplicates, repeated three times. Relative Luminescence Units (RLU) were normalized to percentage values, and sigmoidal concentration-response curves were fitted to the data points using GraphPad Prism 9.5.1 (GraphPad Software, San Diego, CA, USA).

In vivo uterotrophic assay

Based on our results of the in vitro luminometric assay, our aim was to determine the antiestrogenic effect of our test compound in vivo as well. The uterotrophic assay was performed according to the OECD Test Guideline No. 440[33]. 21-day-old female immature Sprague-Dawley rats (weighed 35–47 g) were maintained in an environmentally controlled room under a 12-hour light/dark cycle and were provided tap water and a commercial pellet diet *ad libitum*. Animals were randomly allocated into 5 groups, with 6–7 animals in each group: vehicle (vegetable oil), E2 group (17β-estradiol, 0.1 μg/g), E2 + FULV (0.1 μg/g E2 + 0.3 μg/g fulvestrant), E2 + EDPO (60) (0.1 μg/g E2 + 60 μg/g EDPO), E2 + EDPO (600) (0.1 μg/g E2 + 600 μg/g EDPO). Doses were determined based on literature data on the ED_{50} value of E2 along with our findings established in the in vitro antiestrogenic assay[34]. All chemicals were dissolved or suspended in vegetable oil. Animals were treated once daily for 3 consecutive days by subcutaneous injections according to their recorded body weight. On the fourth day, animals were sacrificed under deep anesthesia (2.5% isoflurane; AErane liquid for inhalation, Baxter Hungary Ltd., Budapest, Hungary), and uterine tissues were surgically removed. Wet uteri were weighed, and the masses of treated tissues were compared to those of positive controls. Our in vivo experiment was permitted by the National Food Chain Safety Office (IV./397/2023).

In vivo allograft study

The 4T1 triple-negative murine breast cancer model was performed as described previously[35]. Briefly, the animal experiments were performed in accordance with animal experimentation and ethics guidelines of the EU (2010/63/EU). Experimental protocols were approved by the responsible governmental agency (National Food Chain Safety Office) in possession of an ethical clearance XXIX./128/2013. Female, 8-10-week-old Charles River-derivative BALB/c mice (Kobay Ltd., Ankara, Turkey) were injected orthotopically with 4T1 breast carcinoma cells (1×10^5 cells suspended in 100 μl serum-free RPMI). The animals had free access to food and water. Ten mice were included in each experimental group. The common vehicle of compounds consisting of 80% Peg-200 and 20% Cremophor EL (BASF, Ludwigshafen, Germany) was dissolved in water for injection at a 1:8 final ratio. After the growth of tumors to an average of 20 mm^3 (on Day 11), animals were randomized into groups. Seven mice per treatment group were treated with 10 μg/g and 30 μg/g of EDPO or buffer placebo daily in 100 μl intraperitoneally for 16 days. Tumors were evaluated macroscopically by the following parameters: (1) incidence of palpable tumors was determined by the daily monitoring of animals in each experimental group; (2) tumor size was measured with a precision caliper and calculated according to the formula: $0.5 \times d^2 \times D$; where d = minor diameter, D = major diameter. Mice showing signs of suffering (loss of > 15% of body weight and/or loss of the righting reflex and/or the inability to eat or drink) due to (ethical) legislation were sacrificed (2.5% isoflurane; AErane liquid for inhalation, Baxter Hungary Ltd., Budapest, Hungary). Animal weights were measured throughout the study to monitor toxicity. Measurement data were evaluated using GraphPad Prism 5.0 (GraphPad, San Diego, CA, USA).

Cell cycle analysis

To determine a possible mechanism of action of EDPO, cell cycle analysis was performed on the ERα+ breast cancer cell line, T47D[36]. Cells were seeded onto 24-well plates at a density of 2.5×10^5 cells/well. After an overnight incubation, cells were treated with EMEM containing an increasing concentration of the test compound (1.75, 3.5 and 7 μM) or fulvestrant (5 μM) for 12, 24, 48 and 72 h. The applied concentrations were based on the previously calculated IC_{50} value of EDPO and literature data[17,37]. Cells were then harvested for centrifugation at 1500 RPM for 10 min at room temperature. The supernatant was removed, and pellets were fixed in cold 70% ethanol. Fixed samples were re-centrifuged and re-suspended and stained in a propidium-iodide (PI) solution, containing 10 μg/mL PI, 10 μg/mL RNase A, and 0.1% sodium citrate, for 30 min in the dark at room temperature. To detect the DNA content of the samples, a CytoFLEX Flow Cytometer bundled with the CytExpert Software (Beckman Coulter, Inc., Indianapolis, IN, USA) was used, where 20,000 events/sample were recorded. The acquired data were evaluated using ModFit LT 3.3.11 software (Verity Software House, Topsham, ME, USA) and GraphPad Prism 5.0. Untreated cells were used as the control group. Apoptotic cells were identified as the hypodiploid (subG1) cell population. Experiments were conducted twice, with four parallel samples for each condition.

Antimigratory (Wound healing) assay

The antimigratory effect of the test compound was determined by utilizing a wound healing assay and specialized wound healing assay chambers (ibidi GmbH, Gräfelfing, Germany)[38]. UPCI-SCC-131 and T47D cells were seeded onto both insert chambers at 35.000 cells/chamber and incubated overnight at previously described

conditions to ensure cell attachment to the microplate surface. The inserts were then gently removed, and the wells were washed twice with 0.5 mL of phosphate-buffered saline (PBS) to remove non-attached cells and debris. Cells were then treated with fresh medium containing 2% FBS and sub-antiproliferative concentrations of the test compound (half of the calculated IC_{50} and IC_{50}, 2.5 and 5 µM for UPCI-SCC-131, 3.5 and 7 µM for T47D cells[17] and were incubated again for 24 and 48 h. The migration of cells toward the wound closure site was visualized using a phase-contrast inverted microscope (Nikon Eclipse TS100 microscope, Nikon Instruments Europe, Amstelveen, The Netherlands). Images were taken for each sample using a CCD camera (QImaging MicroPublisher Color RTV5.0, Teledyne Photometrics, Tucson, AZ, USA) to assess the extent of wound closure. The percentage of cell migration was calculated in treated samples at different intervals (0, 24, and 48 h) by determining cell-free area, and these values were compared with untreated control samples assessed at the same intervals using the ImageJ software (National Institutes of Health, Bethesda, MD, USA). Migration assay experiments were repeated twice with four parallel samples.

Transwell invasion assay

To determine the impact of our test compound on the invasive capacity of T47D cells, we used the Boyden chamber assay. Special chamber inserts with a thin PET membrane covered by a Matrigel basement matrix (BioCoat® Matrigel® Invasion Chambers with 8.0 µm PET Membrane, Corning Inc., Corning, NY, USA) were used. The chambers were rehydrated with serum-free EMEM for 2 h at 37 °C. T47D cell suspensions were prepared in serum-free EMEM with the test compound in sub-antiproliferative concentrations (half of the calculated IC_{50} and IC_{50}, 3.5 and 7 µM[17]) at a density of 2.2×10^5 cells/insert and were seeded into the upper chambers. The lower chambers were filled with EMEM supplemented with 10% FBS to serve as a chemoattractant. Untreated cells were used as negative controls. After a 48-hour incubation period, supernatant and non-invaded cells were removed from the inserts. Cells attached to the bottom of the membrane were gently washed with PBS twice, fixed in ice-cold 96% ethanol, and stained with 1% crystal violet dye for 30 min in the dark. After the dyeing procedure, whole-membrane shots were taken with a microscope fitted with a CCD camera. Images were evaluated using ImageJ, where the sum of the area of invaded cells was compared across treatment groups to determine the invasion rate. Area values were converted to percentages. Experiments were performed twice in duplicates.

Statistical analysis

Statistical evaluation of the results was performed by one-way analysis of variance (ANOVA) followed by Newman-Keuls Multiple Comparison Test using the GraphPad Prism 5.01 or 9.5.1. Data were expressed as mean ± standard error of the mean (SEM) or mean ± standard deviation (SD).

Results

EDPO and fulvestrant display comparable binding profiles to hERα

The atomic resolution structures of the hERα-bound EDPO and 3-BEDPO ligands have not been measured experimentally. However, the elucidation of their binding modes to hERα would be necessary to explain the difference in their antiestrogenic activity. In the present study, computational docking was applied to elucidate the structural basis of the antiestrogenic effects of the ligands. The computational docking procedure was validated on a known experimental structure of hERα LBD in complex with raloxifene (a SERM generally applied in ERα + breast cancer therapy). During the validation the energy-minimized raloxifene was re-docked to the hERα target. It was found that computational docking reproduced the experimental binding mode of raloxifene at high precision of a root mean squared deviation (RMSD) of 1.503 Å, showing the reliability and accuracy of the docking method for this target.

In the next step, the docking of EDPO and 3-BEDPO was performed on the same hERα target, and the calculations resulted in atomic level binding modes of both ligands. For comparison, the binding modes of fulvestrant (an anti-cancer drug targeting hERα also used as a reference molecule in the experiments of the present study) were also mapped by docking. The binding pattern of all docked ligands to hERα is listed residue-wise in Table 2.

The binding patterns of the three ligands (EDPO, 3-BEDPO, fulvestrant) were compared to each other. The steroid parts of EDPO and fulvestrant are stabilized by comparably strong H-bonds with the hERα target residues (E353, R394, and H524). Furthermore, both EDPO and fulvestrant anchored Helix 3 (H3) and Helix 11 (H11) of hERα. EDPO forms H-bonds through its bulky substituent at C16 to T347, while fulvestrant interacts with N532 via its long side-arm at C7. By comparison, 3-BEDPO formed only hydrophobic interactions with the target residues, stronger connections like H-bonds were not established in this case (Fig. 2). Although multiple amino acids within the LBD of hERα have been identified as interacting with all three tested ligands (Table 2), the binding pattern of 3-BEDPO, which lacks antiestrogenic activity, differs significantly from those of EDPO and fulvestrant, both of which exhibit antiestrogenic effects.

EDPO inhibits estrogen-mediated transcriptional activity

To verify our hypothesis, we investigated the antiestrogenic activity of our test compound, EDPO, against fulvestrant using an estrogen-responsive luciferase reporter gene system. To gain insights into the structure-activity relationship of the test compound, we also applied 3-BEDPO in the same concentration range. Transcriptional activity reached its maximum at an E2 concentration of 3.5×10^{-11} M, as determined in preliminary experiments. Calculated concentration values at which the test compounds inhibit 50% of the maximum transcriptional activity of ERα (i.e. IC_{50} values) were 10^{-9} M and 10^{-5} M for fulvestrant and EDPO, respectively. Since 3-BEDPO did not elicit 50% inhibition on the transcriptional activity in the applied concentration range, its IC_{50} value could not be determined (Fig. 3). Our findings suggest that EDPO, unlike

Target residues	Fulvestrant	EDPO	3-BEDPO
L346	x	x	x
T347		x	x
A350	x	x	x
D351	x		
E353	x	x	
W383	x	x	x
L384			x
L387	x	x	x
M388	x		x
R394	x	x	
F404		x	x
M421			x
I424			x
F425			x
L428			x
G521			x
H524	x		x
L525	x	x	x
M528	x		x
S530			x
N532	x		x
V533	x	x	x
V534	x		
P535	x	x	

Table 2. Target residues interacting with ligands within 3.5 Å.

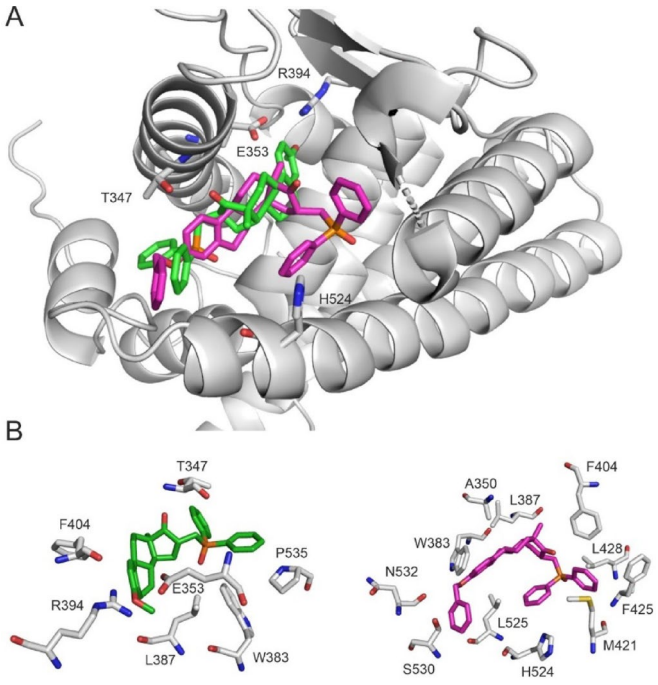

Fig. 2. Differences in the binding modes of EDPO and 3-BEDPO to hERα ligand-binding domain (LBD). (**A**) : Global view of EDPO (green, sticks) and 3-BEDPO (magenta, sticks) binding modes on hERα LBD (grey, cartoon). Target residues E353, R394, T347, and H524 are highlighted with stick representation. (**B**) : Close-up view of EDPO (green, sticks) and 3-BEDPO (magenta, sticks) binding modes on hERα LBD (grey, sticks).

3-BEDPO, acts as an effective antagonist of ERα in a similar, concentration-dependent manner compared to fulvestrant.

EDPO counteracts estrogen-mediated uterine growth

In the current experiment, we demonstrated the antiestrogenic effect of EDPO using a rodent model of the in vivo uterotrophic bioassay. Treatment with E2 alone (100 µg/g) resulted in a 6.6-fold increase in uterine weight compared to the samples in the vehicle (control) group. Fulvestrant (300 µg/g), when co-administered with E2, counteracted the effects of E2 on uterine growth by more than 50%. Similarly to fulvestrant, our test compound mitigated E2-induced uterine growth, in a dose-dependent manner. All changes in uterine weight among the treatment groups were statistically significant compared to the E2-only treatment group. Additionally, uterine weights differed significantly between the E2 + EDPO (60) and the E2 + FULV groups, as well as between the E2 + EDPO (60) and the E2 + EDPO (600) groups. No significant difference was observed between the inhibitory effects on uterine tissue growth of fulvestrant and higher EDPO dose (Fig. 4A). Treatment of the animals resulted in marked visual differences in the uterine tissue between the experimental groups (Fig. 4B). These findings clearly demonstrate that EDPO effectively inhibits ERα-mediated uterine tissue growth in vivo.

EDPO inhibits 4T1 tumor growth in vivo

To determine the in vivo anticancer efficacy of EDPO, the orthotopic and syngeneic 4T1 triple negative breast cancer model was assayed. Throughout the whole 16-day treatment period, a significant and dose-dependent reduction in tumor growth was observed. On Days 10–12 of the treatment period, the test compound in the lower concentration did not exert a significant inhibitory effect on tumor proliferation, meanwhile, the higher dose of EDPO significantly reduced growth from Day 2 onwards (Fig. 5).

EDPO causes G1-phase arrest in T47D cells

To determine the impact of EDPO on cell cycle progression, a propidium iodide-based cell cycle analysis against the T47D cell line was performed. The test compound was applied in an increasing range of concentrations. Fulvestrant (5 µM) was used as a positive control. Throughout the experiments, substantial time- and dose-dependency was observed. Our results indicated cell cycle arrest in the G1 phase, which was evident through the marked increase in the G1 population, accompanied by a corresponding decrease in the S phase population at all investigated time intervals. The EDPO-induced G1 arrest was most pronounced at 24 h of incubation, with a substantial proportion of cells accumulating in the G1 phase at all tested concentrations (Fig. 6).

EDPO reduces migration of UPCI-SCC-131 and T47D cells

To determine the antimigratory effect of EDPO, a wound healing assay was performed on UPCI-SCC-131 and T47D cell lines in a serum-reduced (2% FBS) medium. Cell-free areas were measured by image analysis after 0, 24, and 48 h of incubation with the test compound. Although there is a marked difference in the migratory capacity of the cell lines of interest, EDPO treatment significantly reduced the extent of cell migration both in UPCI-SCC-131 and T47D. In the context of the UPCI-SCC-131 cell line, after 24 h of incubation, the test compound evoked a significant effect at both applied concentrations, however after 48 h of incubation, this effect was observed at the higher concentration only (Fig. 7). Meanwhile, concerning the T47D cell line, changes in the migratory capacity following the treatment were more subtle; nevertheless, remained statistically significant for both concentrations and incubation times (Fig. 8). Our results indicate a substantial, time- and concentration-dependent reduction in the migratory capacity of the investigated tumor cell lines following EDPO treatment.

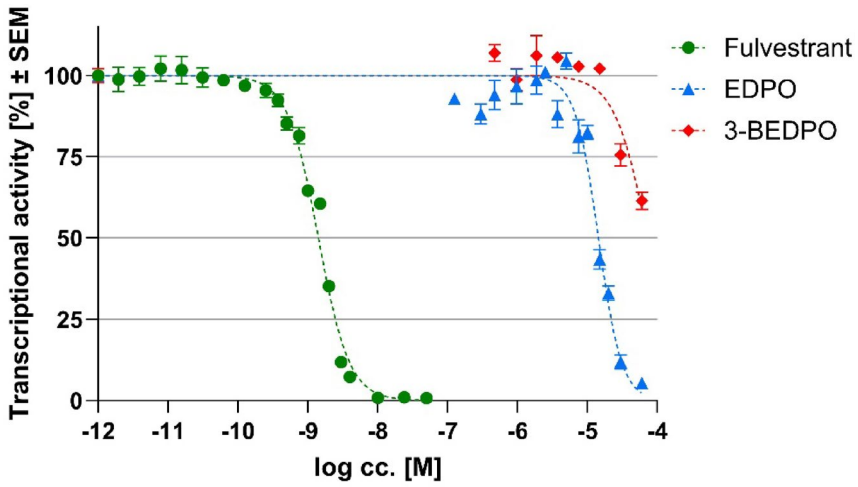

Fig. 3. Concentration-response curves for the inhibition of ERE-Luciferase by fulvestrant, EDPO, and 3-BEDPO. T47D-KBluc cells were treated and co-incubated with 17β-estradiol and the test compounds for 24 h. Data points represent the mean ± SEM of at least three independent experiments.

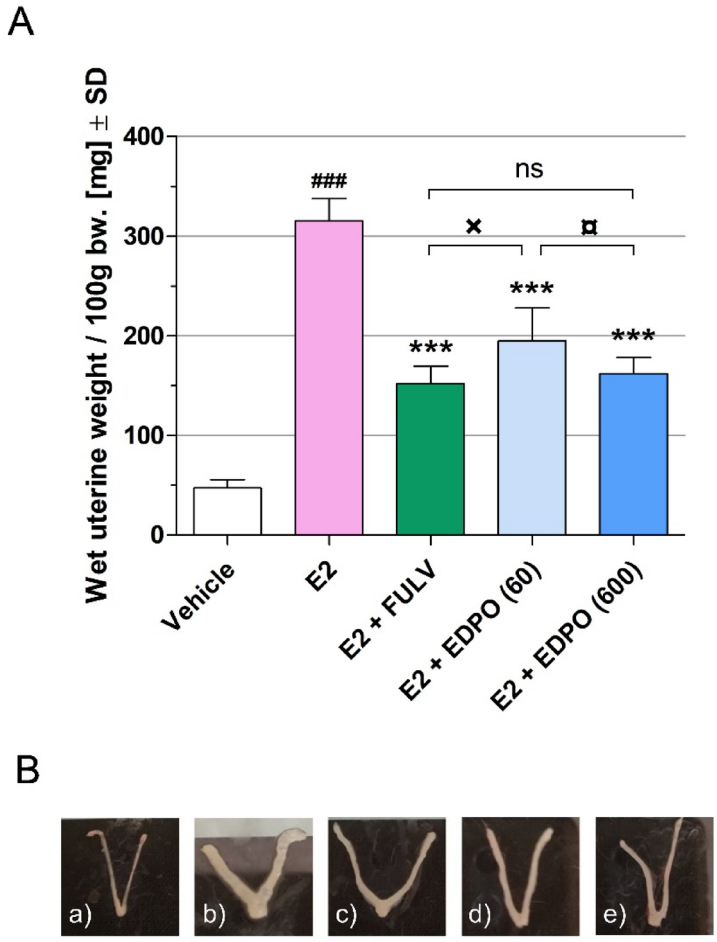

Fig. 4. Effects of fulvestrant and EDPO on uterine weight of female, immature Sprague-Dawley rats. (**A**) : Wet uterine weights are represented as mean ± SD in mg normalized for 100 g of animal body weight. One-way ANOVA was used for statistical analysis, and significant differences are indicated with $^{###}$ at $p < 0.001$ vs. control group; *** at $p < 0.001$ vs. E2 group; × at $p < 0.05$ vs. FULV group; and ¤ at $p < 0.05$ vs. EDPO (600) group; ns: not significant, ($n = 6$). (**B**): Uterine appearances in response to (a) vehicle, (b) E2 (0.1 µg/g), (c) E2 (0.1 µg/g) + FULV (0.3 µg/g), (d) E2 (0.1 µg/g) + EDPO (60 µg/g) and (e) E2 (0.1 µg/g) + EDPO (600 µg/g). Legend: E2: 17β-estradiol; FULV: fulvestrant; EDPO (60): EDPO 60 µg/g; EDPO (600): EDPO 600 µg/g.

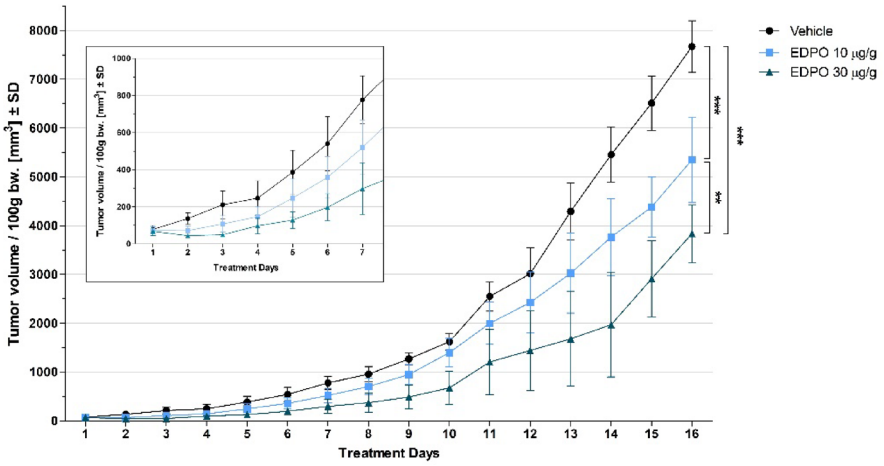

Fig. 5. Effect of EDPO on 4T1 tumor growth in female BALB/c mice. Calculated tumor volumes are represented as mean ± SD mm^3 normalized for 100 g of animal body weight. One-way ANOVA was used for statistical analysis, with ** and *** indicating significance at $p < 0.01$ and $p < 0.001$, respectively. ($n = 7$)

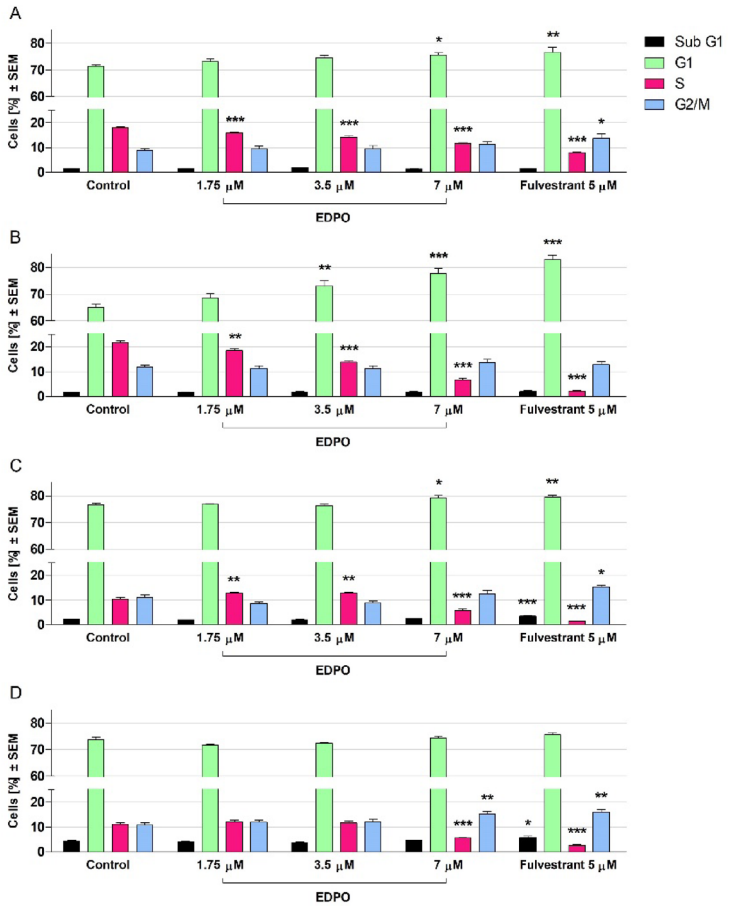

Fig. 6. EDPO-induced cell cycle disturbance in the G1 phase compared to fulvestrant observed after 12 (**A**), 24 (**B**), 48 (**C**), and 72 h (**D**) of incubation on T47D cells. One-way ANOVA was used for statistical analysis, with *, **, and *** indicating significance at $p < 0.05$, $p < 0.01$, and $p < 0.001$, respectively, compared to the non-treated control samples. Results are from at least two independent experiments performed in quadruplicates.

EDPO decreases invasive capacity of T47D cells

To assess the antimetastatic properties of EDPO, a transwell invasion assay using the T47D cell line was performed. Whole-membrane images were taken, where invaded cells were quantified by area. Compared to untreated cells, a significant reduction of the invasive capacity of EDPO-treated cells in both concentrations was observed. The test compound showed a significant anti-invasive effect at both concentrations, reducing the number of invading cells to about 50% compared to the control group, however, this effect did not show significant dose-dependency (Fig. 9).

Discussion

The aim of the present study was to comprehensively evaluate the antiestrogenic and anticancer potential of EDPO, an organophosphorus 13α-estrone derivative, by integrating in silico, in vitro, and in vivo approaches.

In the case of E2 binding to hERα LBD, H12 functioning as a molecular switch is stabilized between H3 and H11 in agonist conformation, meaning that the coactivator-binding pocket remains surface-exposed[39,40], offering a binding site for coactivators. The binding of coactivator peptides is the key step in the signal transduction (transcriptional activation) of hERα for the development of the estrogenic effects[41].

SERMs and SERDs, such as raloxifene and fulvestrant, respectively, contain a steroid-mimicking core or a steroid core that binds to the E2 binding site, along with a long side-arm attached to the B- or D-ring[42]. In the experimental structure of hERα-raloxifene complex, this side-arm creates a stable H-bond with H11, leading to the rearrangement of the coactivator binding pocket. This results in the displacement of H12, which then occupies the coactivator binding side, causing the antiestrogenic effect of the molecule[39,41]. This mechanism was supported by the docking calculation of fulvestrant to hERα LBD. Fulvestrant was stabilized by H-bonds through E353, R394, and H524 - similar to the endogenous E2[39,43] - as well as through N532 on H11 engaging the place of H12. In summary, the docked fulvestrant adopted a conformation and binding pattern similar to that of raloxifene in the experimentally determined atomic-resolution structure.

Based on the docking calculation, the steroid part of EDPO is connected with E353 and R394 through H-bonds (Fig. 2B) similar to other known agonists and antagonists[39,44,45], whereas these interactions are missing in the case of 3-BEDPO (Fig. 2B). Based on analyses of several experimental hERα crystal structures complexed

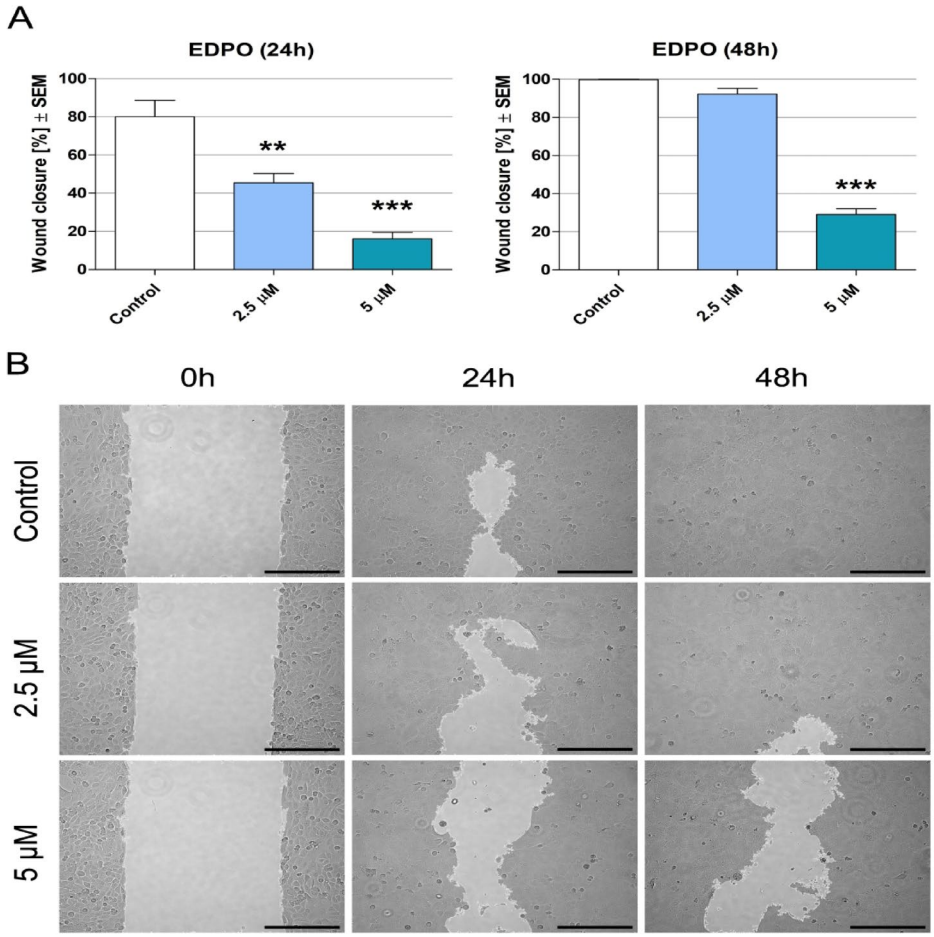

Fig. 7. Antimigratory effect of EDPO measured by wound healing assay. (**A**): Effects of EDPO on UPCI-SCC-131 cell migration after 24 and 48 h of incubation. One-way ANOVA was used for statistical analysis, with ** and *** indicating significance at $p < 0.01$ and $p < 0.001$, respectively, compared to the non-treated control samples. Results are from at least two independent experiments performed in quadruplicates. (**B**): Representative images of the antimigratory effects of EDPO after 0, 24, and 48 h of incubation. Scale bar: 250 µm.

with both agonists and antagonists, it was concluded that formation of H-bond network between the ligand and E353 (on H3), R394 (on H6) residues as well as a water molecule is essential for both types of effects[46]. These interactions are thought to stabilize the complex structure[39,47] *via* an increased inter-helix connection between H3 and H6. The absence of these H-bonds can be seen in the case of low-affinity ligands such as tamoxifen[47], whose metabolite, hydroxy-tamoxifen, with a 100-fold higher affinity, is known to be responsible for the antiestrogenic effect[48,49].

EDPO, exhibiting antiestrogenic activity, also forms a hydrogen bond with T347 in H3 (Fig. 2B), which may prevent H12 from adopting the agonistic conformation. Experimental evidence has shown that ligand interactions with T347 can disrupt the receptor's hydrophobic cluster, thereby destabilizing the conformation required for estrogenic effects[44].

In contrast, 3-BEDPO only forms van der Waals interactions within the binding cavity, which may be insufficient to prevent the necessary protein folding for agonist activity.

Estrogens and ERα play a key role in the development and progression of estrogen receptor-positive breast cancers. Disruption of the ERα signaling pathway at various stages has been proven to be an effective method for mitigating estrogen-induced cell proliferation and metastasis formation. T47D-KBluc cell line has been developed for elucidating the effect of a test compound on the estrogen receptor signaling pathway. The assay revealed that EDPO, similarly to the widely known antiestrogen fulvestrant, undoubtedly inhibits the stimulatory effect of E2 on the downstream transcription of ERE-related genes. 3-BEDPO, the 3-benzyloxy substituted counterpart of EDPO, exhibited a substantially weaker antagonistic effect measured by the luminometric assay, which corresponds with the antiproliferative effectiveness of these compounds on T47D cells.

The uterotrophic assay using the immature rat model is a well-established method for determining (anti) estrogenic activity of drugs in vivo[33]. In the present study, we demonstrated that EDPO mitigates uterine tissue growth when co-administered with E2, in a dose-dependent manner. The reduction in uterine weight highlights

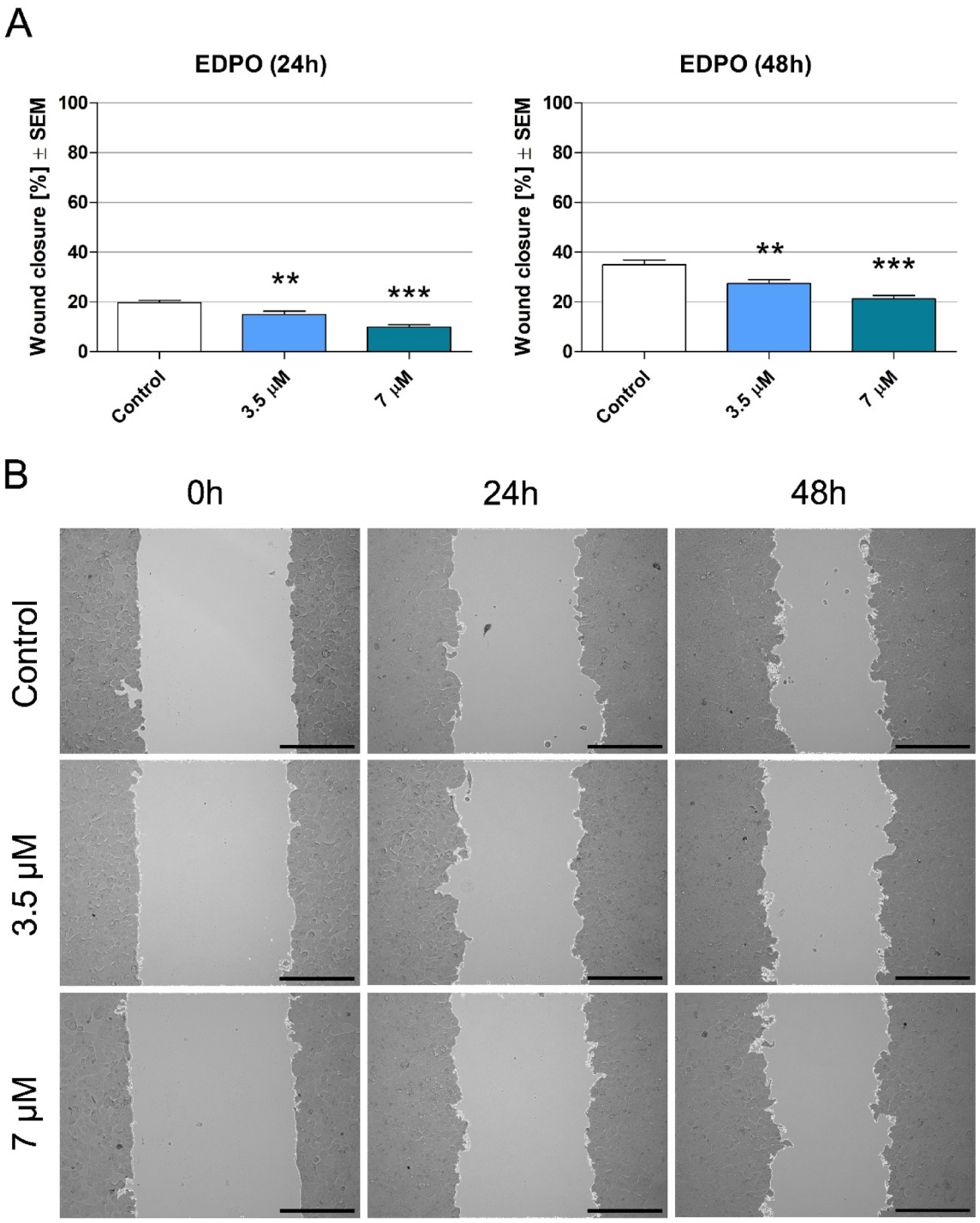

Fig. 8. Antimigratory effect of EDPO measured by wound healing assay. (**A**) : Effects of EDPO on T47D cell migration after 24 and 48 h of incubation. One-way ANOVA was used for statistical analysis, with ** and *** indicating significance at $p < 0.01$ and $p < 0.001$, respectively, compared to the non-treated control samples. Results are from at least two independent experiments performed in quadruplicates. (**B**): Representative images of the antimigratory effects of EDPO after 0, 24, and 48 h of incubation. Scale bar: 250 µm.

EDPO's antagonistic action on ERα in a physiological setting, with efficacy comparable to that of an established chemotherapeutic agent.

Taken together, the results from these complementary methodologies consistently indicate that EDPO interferes with estrogen receptor signaling. The mechanism underlying this antiestrogenic activity may involve a direct competition of E2 and EDPO for binding to ERα, thus interfering with ER-driven transcriptional activation, thereby limiting proliferative signaling in both uterine and hormone-dependent breast cancer tissues. Further receptor binding and gene expression studies are warranted to delineate these mechanisms in detail.

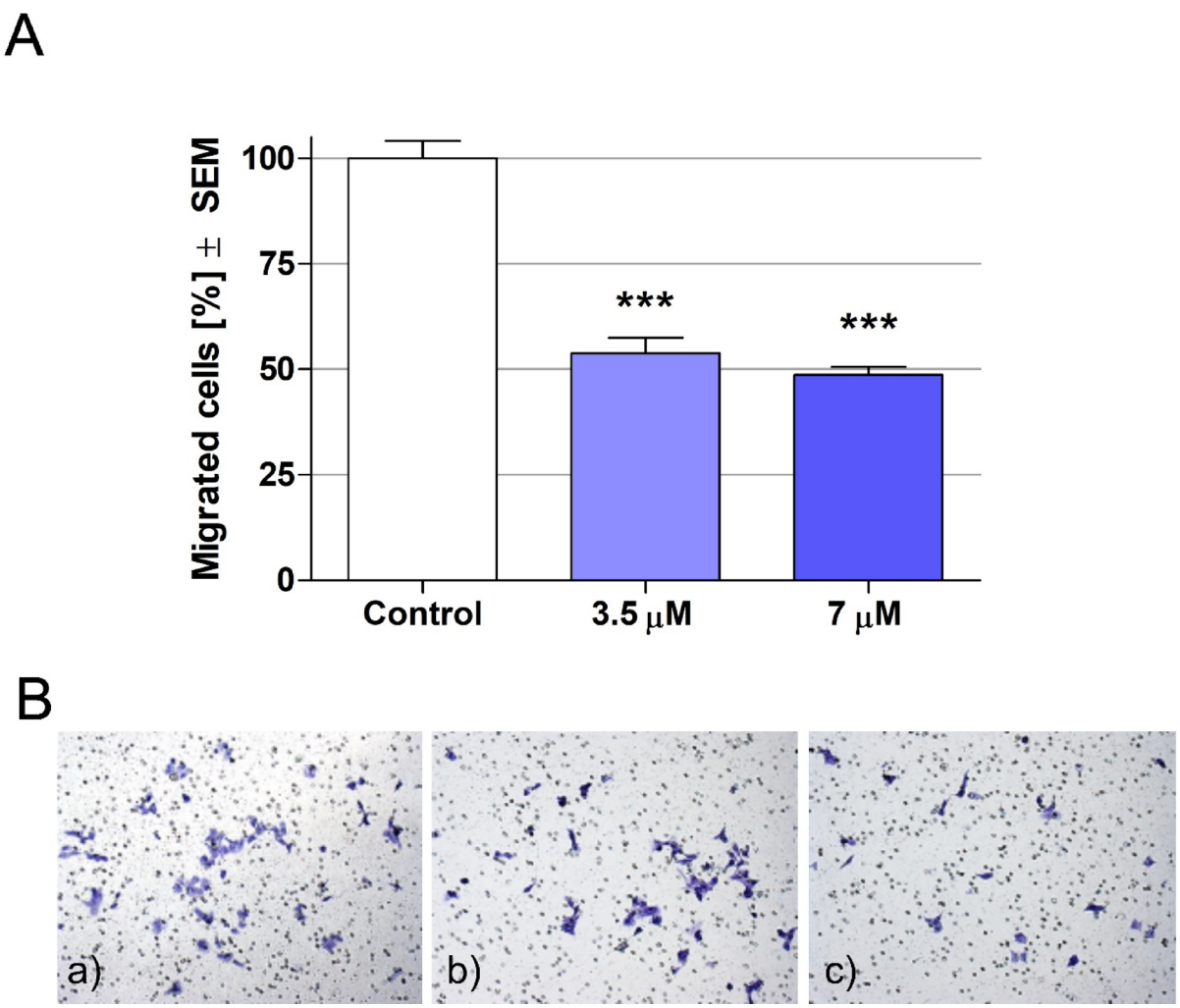

Fig. 9. Effect of EDPO on the invasive capacity of T47D cells measured by transwell migration (Boyden chamber) assay. (**A**) : Effect of EDPO on T47D cell invasion after 48 h of incubation. One-way ANOVA was used for statistical analysis, with *** indicating significance at $p < 0.001$, compared to the non-treated control samples. Results are from at least two independent experiments performed in duplicates. (**B**): Representative images of the non-treated samples (a) and the anti-invasive effects of EDPO at 3.5 μM (b) and 7 μM (c) concentration after a 48-hour incubation period.

It is established that estrogen-induced cell proliferation involves rapid up-regulation of Cyclin D1 and MDM2, and early induction of the proto-oncogene, c-Myc, which are key factors in bypassing the G1/S checkpoint[50–52]. Cyclin D1, in complex with CDK4/6, phosphorylates the retinoblastoma protein (pRb), which, in turn, releases E2F1, consequently activating the transcription of genes essential for S-phase entry, including Cyclin E[53]. Cyclin E then forms an active complex with CDK2, further phosphorylating pRb and reinforcing E2F1 activation[54]. Counterbalancing these proliferative signals, the p53–p21 axis serves as a critical checkpoint. Upon genotoxic stress, p53 transcriptionally activates p21, which inhibits both Cyclin D1-CDK4/6 and Cyclin E-CDK2 complexes. This maintains pRb in its growth-suppressive state and prevents E2F1-mediated G1/S transition[55]. C-Myc facilitates cellular proliferation by directly inhibiting the function of p21, thereby promoting the signaling of cyclin/CDK complexes at the G1/S checkpoint. Furthermore, the human homologue of murine double minute 2 (MDM2), which is generally overexpressed in tumors, is a negative regulator of p53, and accelerates the degradation of pRB and p21. Additionally, MDM2 directly enhances the activity of E2F1[52]. A previous study examined the impact of fulvestrant on MDM2 protein expression and found that it promotes MDM2 protein turnover and downregulation, ultimately causing G1 phase arrest[37]. In our experimental setting, both EDPO and fulvestrant induced substantial G1 phase arrest in T47D cells. This finding along with our previously described results further support our initial hypothesis regarding the antiestrogenic nature of EDPO suggesting that the test compound may disrupt the cell cycle through this mechanism (Fig. 10A).

In ERα+ breast cancer, in addition to its proliferative effect, E2 induces changes in breast cancer cell morphology, enhancing motility and invasion through an ERα-dependent signaling pathway[56]. Mechanistically, activated ERα, through the recruitment of a $G\alpha_i/G\beta\gamma$-signaling, triggers the formation of a multiprotein complex involving ERα, c-Src, phosphoinositide 3-kinase (PI3K), and focal adhesion kinase (FAK), leading

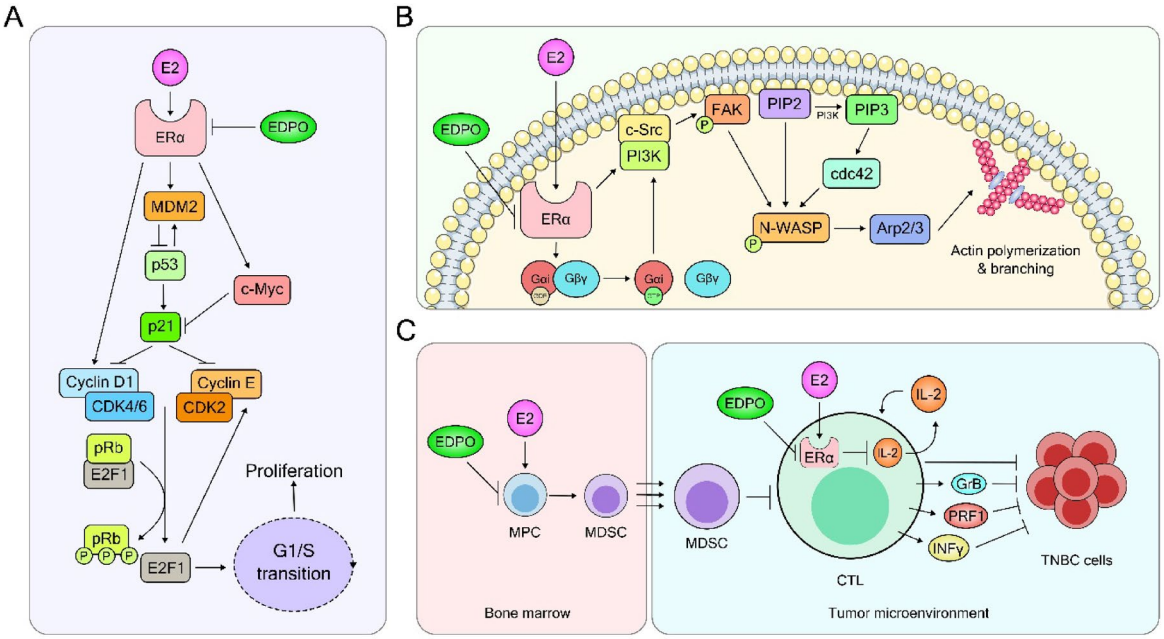

Fig. 10. Proposed mechanism of action of EDPO on ERα+ and triple-negative breast cancer (TNBC) based on experimental and literature data. (**A**): *Antiproliferative effect against ERα+ breast cancer cells.* Estrogen signaling drives G1/S transition by inducing Cyclin D1 and c-Myc, ultimately activating cyclin–CDK complexes to inactivate pRB and release E2F1, while simultaneously suppressing the p53–p21 axis through the induction of MDM2. EDPO may counteract this pathway by blocking ERα-driven transcription, reducing CDK activity, stabilizing p53, and restoring checkpoint control. (**B**): *Antimetastatic effect against ERα+ breast cancer cells.* ERα promotes migration *via* non-genomic signaling: estrogen–ERα activates G-proteins and c-Src, leading to PIP3 generation, FAK-mediated adhesion turnover, and Cdc42/Arp2/3-driven actin remodeling. This cascade reorganizes the cytoskeleton to enhance motility. EDPO is proposed to inhibit this ER-dependent pathway, thereby suppressing cell migration. (**C**): *Antitumor effect against TNBC cells.* Estrogen-induced dual inhibitory action on CTLs through the mobilization of MDSCs and direct blockade of autocrine IL-2 signaling. EDPO is suggested to counteract the effects of E2, thereby shifting the tumor microenvironment toward a pro-immunogenic state and impairing tumor growth. E2: 17β-estradiol; EDPO: [(3-methoxy-17-oxo-13α-estra-1,3,5(10)-trien-16α-yl)methyl]diphenylphosphine oxide; ERα: estrogen receptor alpha; MDM2: murine double minute 2; pRb: retinoblastoma protein; PI3K: phosphoinositide 3-kinase; FAK: focal adhesion kinase; PIP2: phosphatidylinositol 4,5-bisphosphate; PIP3: phosphatidylinositol 4,5,6-trisphosphate; N-WASP: neural Wiskott-Aldrich syndrome protein; Arp2/3: actin related protein 2/3; MPC: myeloid progenitor cell; MDSC: myeloid-derived suppressor cell; CTL: cytotoxic T-lymphocyte; IL-2: interleukin-2; GrB: granzyme B; PRF1: perforin-1; INFγ: interferon-γ. Figures were created in Inkscape v1.4.2 (https://inkscape.org/). Cell membrane image provided by Servier Medical Art (https://smart.servier.com/smart_image/cell-membrane-13/), licensed under CC BY 4.0 (https://creativecommons.org/licenses/by/4.0/).

to FAK phosphorylation, which subsequently activates neural Wiscott-Aldrich syndrome protein (N-WASP). Concurrently, PI3K induces the formation of phosphatidylinositol-3,4,5-trisphosphate (PIP3) which facilitates the recruitment of cdc42. Finally, activated cdc42 in the presence of PIP2, stimulates N-WASP, which then regulates the actin related protein 2/3 (Arp2/3) complex, driving actin branching and membrane remodeling[57] (Fig. 10B). These processes are critical for the movement and dissemination of cancer cells, especially in ERα+ breast cancer. Previous reports have demonstrated that antiestrogens can effectively block the migratory and invasive capabilities of breast cancer cells mediated by ERα[58]. In addition to its expression in breast cancer cells, evidence indicates that ERα is both present and functionally active in HNSCC cell lines, thereby playing a significant role in facilitating their proliferation and invasive characteristics[59].

Given that ERα-mediated FAK phosphorylation and its role in focal adhesion turnover are essential for cancer cell motility, the inhibitory effect of our compound may arise from disrupting these pathways, highlighting its potential as a therapeutic agent to prevent breast cancer and HNSCC progression (Fig. 10B).

It is generally considered that ERα-negative cancers, including triple-negative breast cancers (TNBCs), are unaffected by estrogens. However, findings of recent studies underscore the immunomodulatory effect of estrogens. These discoveries revealed that estrogen signaling plays a pivotal role in tumor progression by creating an immunosuppressive tumor microenvironment (TME), regardless of tumor ERα status[60]. In the bone marrow, E2 drives this process by inducing the differentiation of myeloid progenitor cells into myeloid-derived suppressor cells (MDSCs), which subsequently translocate to the TME and impair the antitumor activity of cytotoxic T lymphocytes (CTLs)[60,61]. Estrogens can also directly inhibit CTLs through the suppression of the autocrine signaling of interleukin-2. In support of this, a recent study employing a 4T1 murine model of TNBC

showed that pharmacological blockade of estrogen signaling with fulvestrant markedly reduced tumor growth, increased CTL infiltration, and shifted the TME toward a pro-immunogenic state, with higher levels of effector molecules like granzyme B, perforin 1, and interferon-γ[61].

Considering the reported findings on the effects of antiestrogens in the 4T1 murine TNBC model, the antitumor activity of EDPO may be attributed to its inhibitory effect on estrogen-dependent immune cells (Fig. 10C).

Conclusions

In the present study, we demonstrate that our test compound, EDPO, exhibits significant antiestrogenic activity, as confirmed through distinct methodologies, which collectively provide compelling evidence of EDPO's antiestrogenic potential. At the molecular level, EDPO induces a specific cell cycle arrest in the investigated breast cancer cell line, a hallmark characteristic of antiestrogens. Beyond its antiestrogenic effects, EDPO displays significant antimetastatic properties, indicating its potency as a therapeutic agent for preventing the dissemination of breast cancer. Additionally, our in vivo experiment utilizing a TNBC model reveals that EDPO effectively suppresses tumor growth, presumably through the inhibition of estrogen-driven immunomodulatory mechanisms. Our findings suggest that the previously reported benefits of antiestrogenic therapies extend beyond their traditional application in classical ERα+ breast cancer. These therapies may also be repurposed to enhance the efficacy of immunotherapy and chemotherapy responses in TNBC and other ERα-negative malignancies by promoting immune infiltration. Collectively, these findings establish EDPO as a promising compound with multifaceted mechanisms of action, warranting further investigation in the development of novel therapeutic strategies for both ERα+ breast cancer and TNBC.

Data availability

All relevant data are available from the corresponding author upon request.

Received: 25 April 2025; Accepted: 6 November 2025
Published online: 22 December 2025

References

1. Bray, F. et al. Global cancer statistics 2022: GLOBOCAN estimates of incidence and mortality worldwide for 36 cancers in 185 countries. *CA Cancer J. Clin.* **74**, 229–263 (2024).
2. Dustin, D., Gu, G. & Fuqua, S. A. W. *ESR1* mutations in breast cancer. *Cancer* **125**, 3714–3728 (2019).
3. Loibl, S. et al. Early breast cancer: ESMO clinical practice guideline for diagnosis, treatment and follow-up. *Ann. Oncol.* **35**, 159–182 (2024).
4. Gennari, A. et al. ESMO clinical practice guideline for the diagnosis, staging and treatment of patients with metastatic breast cancer. *Ann. Oncol.* **32**, 1475–1495 (2021).
5. Dixon, J. M. Endocrine Resistance in Breast Cancer. *New J. Sci.* 1–27 (2014).
6. Wardell, S. E., Nelson, E. R., Chao, C. A. & McDonnell, D. P. Bazedoxifene exhibits antiestrogenic activity in animal models of Tamoxifen-Resistant breast cancer: implications for treatment of advanced disease. *Clin. Cancer Res.* **19**, 2420–2431 (2013).
7. Andreano, K. J. et al. The dysregulated Pharmacology of clinically relevant *ESR1* mutants is normalized by Ligand-activated WT receptor. *Mol. Cancer Ther.* **19**, 1395–1405 (2020).
8. Foster, P. A. Steroid sulphatase and its inhibitors: Past, Present, and future. *Molecules* **26**, 2852 (2021).
9. Osborne, C. K., Wakeling, A. & Nicholson, R. I. Fulvestrant: an oestrogen receptor antagonist with a novel mechanism of action. *Br. J. Cancer*. **90**, S2–S6 (2004).
10. Osborne, C. K., Shou, J., Massarweh, S. & Schiff, R. Crosstalk between Estrogen receptor and growth factor receptor pathways as a cause for endocrine therapy resistance in breast cancer. *Clin. Cancer Res. Off J. Am. Assoc. Cancer Res.* **11**, 865s–70s (2005).
11. Liu, J. et al. Fulvestrant-3 boronic acid (ZB716): an orally bioavailable selective Estrogen receptor downregulator (SERD). *J. Med. Chem.* **59**, 8134–8140 (2016).
12. Garner, F., Shomali, M., Paquin, D., Lyttle, C. R. & Hattersley, G. RAD1901: a novel, orally bioavailable selective Estrogen receptor degrader that demonstrates antitumor activity in breast cancer xenograft models. *Anticancer Drugs*. **26**, 948–956 (2015).
13. El-Ahmad, Y. et al. Discovery of 6-(2,4-Dichlorophenyl)-5-[4-[(3 *S*)-1-(3-fluoropropyl)pyrrolidin-3-yl]oxyphenyl]-8,9-dihydro-7 *H* -benzo[7]annulene-2-carboxylic acid (SAR439859), a potent and selective Estrogen receptor degrader (SERD) for the treatment of Estrogen-Receptor-Positive breast cancer. *J. Med. Chem.* **63**, 512–528 (2020).
14. Liang, J. et al. GDC-9545 (Giredestrant): A potent and orally bioavailable selective Estrogen receptor antagonist and degrader with an exceptional preclinical profile for ER + Breast cancer. *J. Med. Chem.* **64**, 11841–11856 (2021).
15. Scott, J. S. et al. Discovery of AZD9833, a potent and orally bioavailable selective Estrogen receptor degrader and antagonist. *J. Med. Chem.* **63**, 14530–14559 (2020).
16. Bhagwat, S. V. et al. Preclinical characterization of LY3484356, a novel, potent and orally bioavailable selective Estrogen receptor degrader (SERD). *Cancer Res.* **81**, 1236–1236 (2021).
17. Mernyák, E. et al. Microwave-assisted Phospha-Michael addition reactions in the 13α-oestrone series and *in vitro* antiproliferative properties. *J. Enzyme Inhib. Med. Chem.* **36**, 1931–1937 (2021).
18. Ayan, D., Roy, J., Maltais, R. & Poirier, D. Impact of estradiol structural modifications (18-methyl and/or 17-hydroxy inversion of configuration) on the in vitro and in vivo estrogenic activity. *J. Steroid Biochem. Mol. Biol.* **127**, 324–330 (2011).
19. Mernyák, E. et al. Synthesis of trans-16-triazolyl-13α-methyl-17-estradiol diastereomers and the effects of structural modifications on their in vitro antiproliferative activities. *J. Steroid Biochem. Mol. Biol.* **150**, 123–134 (2015).
20. Szabó, J. et al. Synthesis and biological evaluation of 13α-estrone derivatives as potential antiproliferative agents. *Steroids* **113**, 14–21 (2016).
21. Bacsa, I. et al. Synthesis of novel 13α-estrone derivatives by Sonogashira coupling as potential 17β-HSD1 inhibitors. *Beilstein J. Org. Chem.* **13**, 1303–1309 (2017).
22. Bacsa, I. et al. Synthesis and structure–activity relationships of 2- and/or 4-halogenated 13β- and 13α-estrone derivatives as enzyme inhibitors of Estrogen biosynthesis. *J. Enzyme Inhib. Med. Chem.* **33**, 1271–1282 (2018).
23. Jójárt, R. et al. Pd-Catalyzed microwave-assisted synthesis of phosphonated 13α-estrones as potential OATP2B1, 17β-HSD1 and/or STS inhibitors. *Beilstein J. Org. Chem.* **14**, 2838–2845 (2018).
24. Berman, H. M. The protein data bank. *Nucleic Acids Res.* **28**, 235–242 (2000).

25. Hosfield, D. et al. (ed, J.) Stereospecific Lasofoxifene derivatives reveal the interplay between Estrogen receptor alpha stability and antagonistic activity in ESR1 mutant breast cancer cells. *eLife* **11** e72512 (2022).
26. Morisseau, C., Pakhomova, S., Hwang, S. H., Newcomer, M. E. & Hammock, B. D. Inhibition of soluble epoxide hydrolase by fulvestrant and sulfoxides. *Bioorg. Med. Chem. Lett.* **23**, 3818–3821 (2013).
27. Stewart, J. J. P. Optimization of parameters for semiempirical methods VI: more modifications to the NDDO approximations and re-optimization of parameters. *J. Mol. Model.* **19**, 1–32 (2013).
28. Abraham, M. J. et al. High performance molecular simulations through multi-level parallelism from laptops to supercomputers. *SoftwareX 1–2*. **GROMACS**, 19–25 (2015).
29. Lindorff-Larsen, K. et al. Improved side-chain torsion potentials for the amber ff99SB protein force field. *Proteins Struct. Funct. Bioinforma*. **78**, 1950–1958 (2010).
30. Mark, P. & Nilsson, L. Structure and dynamics of the TIP3P, SPC, and SPC/E water models at 298 K. *J. Phys. Chem. A*. **105**, 9954–9960 (2001).
31. Morris, G. M. et al. AutoDock4 and AutoDockTools4: automated Docking with selective receptor flexibility. *J. Comput. Chem.* **30**, 2785–2791 (2009).
32. Wilson, V. S. Development and characterization of a cell line that stably expresses an Estrogen-Responsive luciferase reporter for the detection of Estrogen receptor agonist and antagonists. *Toxicol. Sci.* **81**, 69–77 (2004).
33. OECD. Test No. 440: Uterotrophic Bioassay in Rodents: A Short-Term Screening Test for Oestrogenic Properties. OECD, (2007). https://doi.org/10.1787/9789264067417-en
34. Wakeling, A. E. & Bowler, J. ICI 182,780, a new antioestrogen with clinical potential. *J. Steroid Biochem. Mol. Biol.* **43**, 173–177 (1992).
35. Balog, J. Á. et al. Single cell mass cytometry revealed the Immunomodulatory effect of cisplatin via downregulation of Splenic CD44+, IL-17A + MDSCs and promotion of Circulating IFN-γ + Myeloid cells in the 4T1 metastatic breast cancer model. *Int. J. Mol. Sci.* **21**, 170 (2019).
36. Vermes, I., Haanen, C. & Reutelingsperger, C. Flow cytometry of apoptotic cell death. *J. Immunol. Methods*. **243**, 167–190 (2000).
37. Dolfi, S. C. et al. Fulvestrant treatment alters MDM2 protein turnover and sensitivity of human breast carcinoma cells to chemotherapeutic drugs. *Cancer Lett.* **350**, 52–60 (2014).
38. Behrens, J., Kameritsch, P., Wallner, S., Pohl, U. & Pogoda, K. The carboxyl tail of Cx43 augments p38 mediated cell migration in a gap junction-independent manner. *Eur. J. Cell. Biol.* **89**, 828–838 (2010).
39. Brzozowski, A. M. et al. Molecular basis of agonism and antagonism in the oestrogen receptor. *Nature* **389**, 753–758 (1997).
40. Arao, Y. & Korach, K. S. The physiological role of Estrogen receptor functional domains. *Essays Biochem.* **65**, 867–875 (2021).
41. Nettles, K. W. & Greene, G. L. Ligand control of coregulator recruitment to nuclear receptors. *Annu. Rev. Physiol.* **67**, 309–333 (2005).
42. Hancock, G. R. et al. Unconventional isoquinoline-based serms elicit fulvestrant-like transcriptional programs in ER + breast cancer cells. *Npj Breast Cancer*. **8**, 130 (2022).
43. Traboulsi, T., El Ezzy, M., Gleason, J. L. & Mader, S. Antiestrogens: structure-activity relationships and use in breast cancer treatment. *J. Mol. Endocrinol.* **58**, R15–R31 (2017).
44. Delfosse, V. et al. Structural and mechanistic insights into bisphenols action provide guidelines for risk assessment and discovery of bisphenol A substitutes. *Proc. Natl. Acad. Sci.* **109**, 14930–14935 (2012).
45. Shiau, A. K. et al. The structural basis of Estrogen Receptor/Coactivator recognition and the antagonism of this interaction by Tamoxifen. *Cell* **95**, 927–937 (1998).
46. Gajadeera, N. & Hanson, R. N. Review of fluorescent steroidal ligands for the Estrogen receptor 1995–2018. *Steroids* **144**, 30–46 (2019).
47. Gao, L., Tu, Y. & Eriksson, L. A. More Stable, more estrogenic: the SERM-ERα LBD complex. *J. Biophys. Chem.* **02**, 233–243 (2011).
48. Coezy, E., Borgna, J. L. & Rochefort, H. Tamoxifen and metabolites in MCF7 cells: correlation between binding to Estrogen receptor and Inhibition of cell growth. *Cancer Res.* **42**, 317–323 (1982).
49. Johnson, M. D. et al. Pharmacological characterization of 4-hydroxy-N-desmethyl Tamoxifen, a novel active metabolite of Tamoxifen. *Breast Cancer Res. Treat.* **85**, 151–159 (2004).
50. Prall, O. W. J., Sarcevic, B., Musgrove, E. A., Watts, C. K. W. & Sutherland, R. L. Estrogen-induced activation of Cdk4 and Cdk2 during G1-S phase progression is accompanied by increased Cyclin D1 expression and decreased Cyclin-dependent kinase inhibitor association with Cyclin E-Cdk2. *J. Biol. Chem.* **272**, 10882–10894 (1997).
51. Swetzig, W. M., Wang, J. & Das, G. M. Estrogen receptor alpha (ERα/ESR1) mediates the p53-independent overexpression of MDM4/MDMX and MDM2 in human breast cancer. *Oncotarget* **7**, 16049–16069 (2016).
52. Martin, K. et al. Stimulation of E2F1/DP1 transcriptional activity by MDM2 oncoprotein. *Nature* **375**, 691–694 (1995).
53. Caldon, C. E. et al. Estrogen regulation of Cyclin E2 requires Cyclin D1 but not c-Myc. *Mol. Cell. Biol.* **29**, 4623–4639 (2009).
54. Akiyama, T., Ohuchi, T., Sumida, S., Matsumoto, K. & Toyoshima, K. Phosphorylation of the retinoblastoma protein by cdk2. *Proc. Natl. Acad. Sci.* **89**, 7900–7904 (1992).
55. Engeland, K. Cell cycle regulation: p53-p21-RB signaling. *Cell. Death Differ.* **29**, 946–960 (2022).
56. Giretti, M. S. et al. Extra-Nuclear signalling of Estrogen receptor to breast cancer cytoskeletal Remodelling, migration and invasion. *PLoS ONE*. **3**, e2238 (2008).
57. Sanchez, A. M. et al. Estrogen Receptor-α promotes breast cancer cell motility and invasion via focal adhesion kinase and N-WASP. *Mol. Endocrinol.* **24**, 2114–2125 (2010).
58. Rajah, T. T. et al. Influence of antiestrogens on NIH-3T3-Fibroblast-Induced motility of breast cancer cells. *Chemotherapy* **47**, 56–69 (2001).
59. Egloff, A. M. et al. Cross-Talk between Estrogen receptor and epidermal growth factor receptor in head and neck squamous cell carcinoma. *Clin. Cancer Res.* **15**, 6529–6540 (2009).
60. Svoronos, N. et al. Tumor Cell–Independent Estrogen signaling drives disease progression through mobilization of Myeloid-Derived suppressor cells. *Cancer Discov.*. **7**, 72–85 (2017).
61. Kajihara, N., Ge, Y. & Seino, K. Blocking of oestrogen signals improves anti-tumour effect regardless of oestrogen receptor alpha expression in cancer cells. *Br. J. Cancer*. **129**, 935–946 (2023).

Acknowledgements

We acknowledge the Digital Government Development and Project Management Ltd. for awarding us access to the Komondor HPC facility based in Hungary. The authors thank Károly Nagy for his technical assistance.

Author contributions

S.B. : Investigation, Formal analysis, Writing – original draft. **P.G.** : Methodology, Investigation, Conceptualization. **N.B.** : Methodology, Investigation. **L.G.P.** : Investigation, Methodology, Formal analysis, Writing – original draft. **R.B.** : Investigation, Formal analysis, Writing – original draft. **C.H.** : Software, Supervision, Writing – review & editing. **I.Z.** : Resources, Funding acquisition, Conceptualization, Writing

– review & editing. **E.M.** : Conceptualization, Methodology, Writing – review & editing. **R.M.** : Conceptualization, Resources, Supervision, Writing – review & editing.

Funding
This study was supported by the János Bolyai Research Scholarship of the Hungarian Academy of Sciences. Project no TKP2021-EGA-32 has been implemented with the support provided by the Ministry of Culture and Innovation of Hungary from the National Research, Development and Innovation Fund, financed under the TKP2021-EGA funding scheme. This work was funded by the Hungarian National Science and Research Fund (OTKA) grant No. 143690 and and SNN 139323 and University of Szeged Open Access Fund, Grant ID 7727.

Declarations

Competing interests
The authors declare no competing interests.

Ethics approval
Animal experiments were designed, carried out and evaluated as described in ARRIVE guidelines.

Additional information
Correspondence and requests for materials should be addressed to R.M.